論文 / 著書情報
Article / Book Information

Title	Simple Fluorogenic Cellular Assay for Histone Deacetylase Inhibitors Based on Split-Yellow Fluorescent Protein and Intrabodies
Authors	Yuki Ohmuro-Matsuyama, Tetsuya Kitaguchi, Hiroshi Kimura, Hiroshi Ueda
Citation	ACS Omega, vol. 6, Issue 15, p. 10039-10046
Pub. date	2021, 4
DOI	http://dx.doi.org/10.1021/acsomega.0c06281

ACS OMEGA

http://pubs.acs.org/journal/acsodf

Article

Simple Fluorogenic Cellular Assay for Histone Deacetylase Inhibitors Based on Split-Yellow Fluorescent Protein and Intrabodies

Yuki Ohmuro-Matsuyama, Tetsuya Kitaguchi, Hiroshi Kimura, and Hiroshi Ueda*

Cite This: *ACS Omega* 2021, 6, 10039−10046

Read Online

ACCESS | Metrics & More | Article Recommendations | Supporting Information

ABSTRACT: Histone deacetylase (HDAC) inhibitors that regulate the posttranslational modifications of histone tails are therapeutic drugs for many diseases such as cancers, neurodegenerative diseases, and asthma; however, convenient and sensitive methods to measure the effect of HDAC inhibitors in cultured mammalian cells remain limited. In this study, a fluorogenic assay was developed to detect the acetylation of lysine 9 on histone H3 (H3K9ac), which is involved in several cancers, Alzheimer's disease, and autism spectrum disorder. To monitor the changes in H3K9ac levels, an H3K9ac-specific intrabody fused with a small fragment FP11 of the split-yellow fluorescent protein (YFP) (scFv-FP11) was expressed in mammalian cells, together with a larger YFP fragment FP1-10 fused with a nuclear localization signal. When the intranuclear level of H3K9ac is increased, the scFv-FP11 is more enriched in the nucleus via passive diffusion through the nuclear pores from the cytoplasm, which increases the chance of forming a fluorescent complex with the nuclear YFP1-10. The results showed that the YFP fluorescence increased when the cells were treated with HDAC inhibitors. Moreover, the sensitivity of the split YFP reporter system to three HDAC inhibitors was higher than that of a conventional cell viability test. The assay system will be a simple and sensitive detection method to evaluate HDAC inhibitor activities at the levels of both single cells and cell populations.

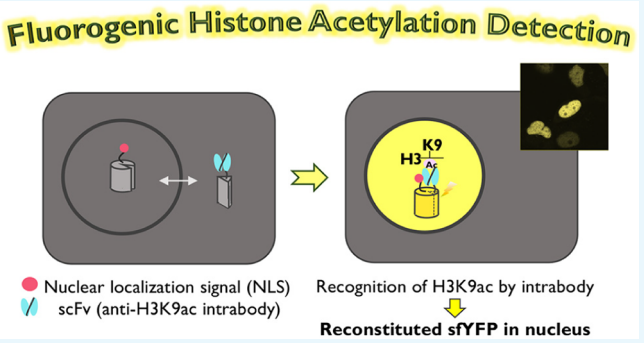

INTRODUCTION

Many factors such as obesity, stress, smoking, allergens, and environmental pollutants have been recently reported to promote anomalous posttranslational histone modifications, which can induce the unbalanced expression of specific genes and lead to many diseases including cancers,[1−7] neurodegenerative diseases,[5,8−11] asthma,[11−15] and bone fluorosis.[16−19] Hyperacetylation of lysine 9 on histone 3 (H3K9ac) was observed in cancers in the lungs,[7] breast,[5] liver,[4] colon,[1] and stomach,[6] as well as in neurodegenerative diseases such as Alzheimer's disease[8,20,21] and autism spectrum disorder.[21] Histone deacetylase (HDAC) inhibitors have therefore been developed as therapeutic agents for these diseases.[15,22,23]

The effect of HDAC inhibitors are typically analyzed by the number of living and dead cells in medical science and by western blotting and chromatin immunoprecipitation assays in cell biology. Recently, several methods were developed to measure histone acetylation in living cells, including fluorescence resonance energy transfer (FRET)-based probes and antibody binding-based probes.[24,25] Intramolecular FRET probes have been developed using a pair of cyan fluorescent protein (CFP) and yellow fluorescent protein (YFP) connected through a histone and an acetyl-binding protein domain. The acetylation on the histone moiety induces an intramolecular structural change to affect the FRET efficiency. So far, FRET probes for histone H3K9/K14, H4K12, and H4 hyperacetylation have been used to monitor the effects of small chemical inhibitors.[26] However, these methods could not detect intrinsically acetylated histones or H3K9 acetylation specifically. Apart from FRET probes, antibody binding-based probes that can detect endogenous and site-specific histone acetylation have been reported.[27,28]

To explore antibody-based probes that can be expressed inside the cells, stable antibodies called "intrabodies," which can retain robust structures even in the reducing environment of the cytoplasm and nucleus, were used.[29] Sato et al. generated an scFv intrabody, which specifically recognizes H3K9ac in the cells.[30,31] When the specific intrabody fused with green fluorescent protein (GFP), named "mintbody," was expressed in the cell, it was mainly distributed in the cytoplasm without disturbing the cell growth. Increased H3K9 acetylation in the nucleus by an HDAC inhibitor resulted in the

Received: December 26, 2020
Accepted: March 31, 2021
Published: April 7, 2021

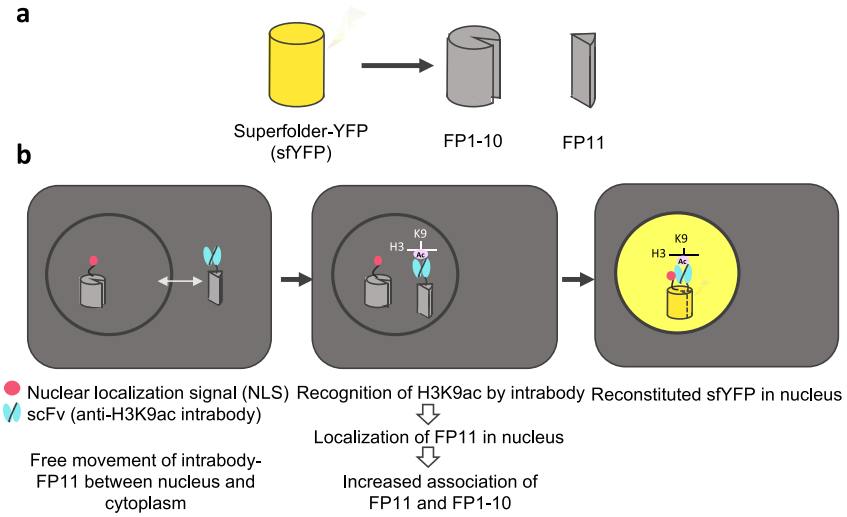

Figure 1. Probe design strategy. (a) Scheme for the split sfYFP system. An sfYFP was separated into two fragments, FP1-10 (the region from the N-terminus to the 10th) and FP11 (the last 11th β-sheet strand). (b) Scheme for the fluorogenic detection of H3K9ac.

redistribution of mintbodies to the nucleus. Similarly, H4K20 mono-methylation was also successfully observed.[32] Based on this mintbody technology, we have recently developed an FRET-type probe for H3K9ac,[33] in which a CFP variant SeCFP and a YFP variant YPet were fused to the N- and C-termini of the intrabody, respectively. Binding of the probe to H3K9ac induces a conformational change in the intrabody, which results in increased FRET efficiency. While these intrabody-based probes have their own merits, they also have limitations. The fluorescence intensity of mintbodies in the nucleus needs to be manually compared with that in the cytoplasm, while the FRET-based probes require the measurements of both cyan and yellow fluorescence, and their dynamic range was rather narrow.

To address these limitations and create a better method to screen HDAC inhibitors, a new intrabody-based fluorogenic probe was constructed with the split-fluorescent protein (FP) system composed of two fragments FP1-10 and FP11 of the superfolder YFP (sfYFP).[34] The advantages of this system include the simplicity of only measuring the single-color fluorescence intensity and the wide dynamic range suitable for capturing weak transient interactions.[35−37] In addition, the relatively small FP11 sequence minimizes perturbations to the folding and binding of the fusion partner.[38,39]

RESULTS

In the split-YFP system, the gene for sfYFP was separated into two fragments, FP1-10 (the region from the N-terminus to the 10th) and FP11 (the 11th β-sheet strand) (Figure 1a). In this study, FP1-10 was fused to the NLS derived from the SV40 large T-antigen, and FP11 was fused to the scFv intrabody. The assay scheme is described as follows: (1) When NLS-FP10 and scFv-FP11 are coexpressed in the cells, NLS-FP1-10 can pass through the nuclear pores by diffusion and accumulates in nuclei. (2) As scFv-FP11 shuttles between the nucleus and the cytoplasm, the level of scFv-FP11 nuclear localization is positively correlated with that of H3K9 acetylation. (3) With increased scFv-FP11 abundance in the nucleus, the chance of FP1-10 binding to FP11 would increase, resulting in sfYFP reconstitution and increased YFP signals (Figure 1b). This will enable simpler assessment of HDAC inhibitor activities.

We have previously made an FRET-based probe using the same scFv. In this study, two vectors for intrabody-based probes, FP11-scFv-CFP and CFP-scFv-FP11, were constructed by modifying the FRET-based probe. Also, an expression vector for NLS-FP1-10 was made to express this protein in the nucleus. Notably, the FP11 in the former two probes complements the FP1-10 of sfYFP to form fluorescent sfYFP. However, because of its stronger yellow fluorescence and lower aggregation, CFP-scFv-FP11 was used hereafter. When CFP-scFv-FP11 was expressed together with NLS-FP1-10 in Cos-7 cells, the YFP signals in the nuclei was clearly increased by trichostatin A (TSA) treatment (Figure 2a). Similar results were observed using U2OS cells (Figure 2b).

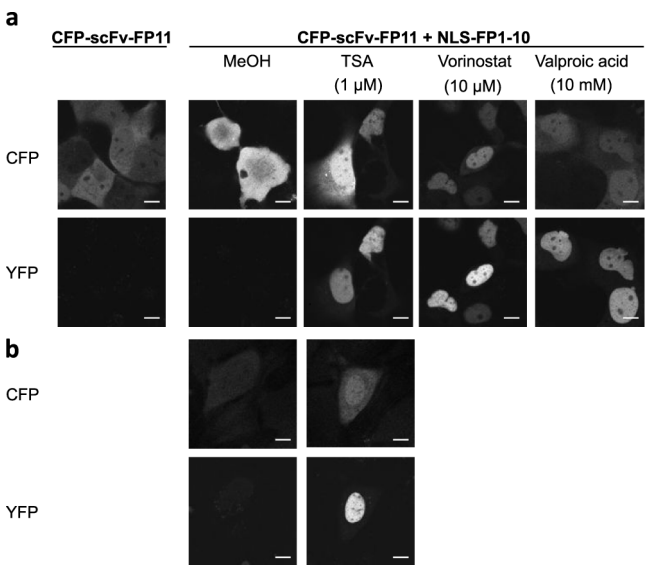

Figure 2. Observation of YFP signals in the nuclei induced by HDAC inhibitor treatments by confocal microscopy. Cos-7 (a) and U2OS (b) cells were transfected with CFP-scFv-FP11 without or with NLS-FP1-10, left for 5 h, and incubated with HDAC inhibitors for 22−25 h before image acquisition. sfYFP was reconstituted from the pairing of FP1-10 and CFP-scFv-FP11 in the nuclei when the cells were treated with HDAC inhibitors TSA, vorinostat, valproic acid, or 0.1% MeOH as a negative control. Scale bar: 5 μm.

https://doi.org/10.1021/acsomega.0c06281
ACS Omega 2021, 6, 10039−10046

When Cos-7 cells expressing CFP-scFv-FP11 and FP1-10 were treated with the other two HDAC inhibitors vorinostat and valproic acid, increased levels of YFP signals in the nuclei were observed (Figure 2a). As TSA was more effective than vorinostat and valproic acid, consistent with previous studies,[43−45] we used TSA in the following analysis.

To compare the localization of the probes with H3K9ac, Cos-7 cells expressing CFP-scFv-FP11 and NLS-FP1-10 were fixed and stained with Cy5-labeled anti-H3K9ac antibody. As seen in Figure 3, TSA treatment increased both CFP and YFP

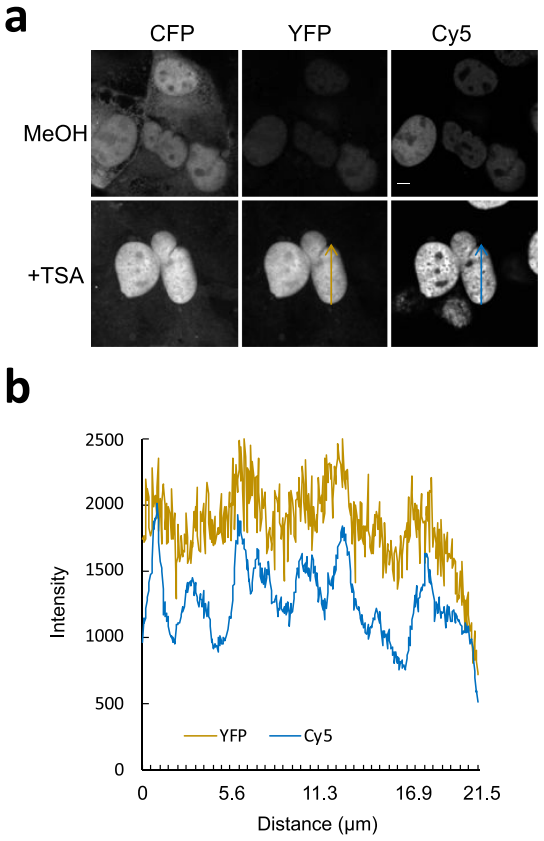

Figure 3. Confocal microscopic analysis of Cos-7 cells expressing CFP-scFv-FP11 and NLS-FP1-10. Four hours after transfection, the cells were incubated with the vehicle (MeOH) or 1 μM TSA for 16 h, before fixation and staining with Cy5-labeled anti-H3K9ac antibody. (a) Single confocal sections for CFP, YFP, and Cy5 are shown. (b) Line intensity profiles are shown. Scale bar: 4 μm.

signals in nuclei. Line profiles showed that YFP and H3K9ac were concentrated in the same regions, although YFP was more diffusely distributed than anti-H3K9ac antibody, probably due to the dynamic binding of the probe to the target. These data support the view that CFP-scFv-FP11 binds to H3K9ac to increase the nuclear retention period to allow forming the YFP-fluorescing complex with NLS-FP1-10.

To attain further insight into this hypothesis, we compared the YFP signal intensity in the control (MeOH) and TSA-treated samples using the CFP intensity as a reference using the images like the one used for Figure 3a (Figure S1). This is because it will at least partly compensate the effect of the probe expression levels, namely, that of CFP-scFv-FP11. After manually selecting nuclear and whole cellular regions in the pictures and quantifying the YFP and CFP fluorescence intensities, respectively, the TSA-dependent fluorescence intensity ratio was found to increase to more than 2.5-fold at 1 μM, confirming that a higher signal is generated by our YFP reconstitution system.

To further confirm the microscopic observations, a larger number of Cos-7 cells were analyzed by flow cytometry. As expected, HDAC inhibitors substantially enhanced YFP signals in the cells (Figures 4 and S2). The expression levels of the probes, CFP-scFv-FP11 and NLS-FP1-10, were also examined by western blotting (Figure S3). The two bands of NLS-FP1-10 were detected, which could be due to its cleavage and/or modification.[46−48] TSA treatment appeared to have slightly increased the level of CFP-scFv-FP11, while other HDAC inhibitors had little effect, suggesting that the increased YFP signals and the increased number of YFP-positive cells were mainly caused by the increased levels of H3K9 acetylation.

Although the CFP in scFv-FP11 probes was useful to track and measure their expression levels, the aggregation of sfYFP in the nuclei was sometimes observed. Hence, the APP-tag derived from the acidic intrinsically disordered region of APP was used instead of CFP because the APP-tag was shown to promote the folding of the fusion partners.[49] FP11-scFv-APP and APP-scFv-FP11 plasmids were expressed in Cos-7 cells together with NLS-FP1-10. TSA treatment induced higher YFP signals in the nuclei of cells expressing both pairs, FP11-scFv-APP and NLS-FP1-10, as well as APP-scFv-FP11 and NLS-FP1-10 (Figure S4). However, the background signals of the latter pair were significantly lower. In addition, 2 days after the transfection, several cells expressing FP11-scFv-APP showed substantial fluorescent signals in the nuclei (Figure S4, arrows), whereas the cells expressing APP-scFv-FP11 did not show intense nuclear signals. Therefore, APP-scFv-FP11 was chosen as the probe for subsequent analyses.

One day after the transfection of APP-scFv-FP11 and FP1-10, the cells were either untreated (control, 0.1% MeOH) or treated with three HDAC inhibitors TSA, vorinostat, and valproic acid. In contrast to the control group that showed little fluorescence, intense nuclear signals were observed in the cells treated with HDAC inhibitors (Figure 5). This result was confirmed by flow cytometry (Figure 6), in which the fractions of cells emitting YFP signals were increased by all HDAC inhibitors. In addition, HDAC inhibitors produced substantial fractions of smaller damaged cells (Figure 6a). The proportions of the cells with YFP signals and the damaged cells were positively correlated with the concentrations of HDAC inhibitors (Figures 6b and S5). When the cells were treated with 100 nM TSA, 1 μM vorinostat, or 1 mM valproic acid, the fractions of damaged cells did not significantly increase compared to those of other concentrations; however, those cells with YFP signals remarkably increased, showing the superior sensitivity of the detection method.

DISCUSSION

In this study, we reported a sensitive and robust method of assessing HDAC inhibitor activities on H3K9 acetylation. Unlike the mintbodies and the FRET-based probes that reversibly monitor the acetylation levels, the newly developed split FP system is less reversible because once sfYFP is reconstituted from FP11 and FP1-10, it is not easily separated. Therefore, this new method might not be able to effectively detect dynamic acetylation and deacetylation under physiological conditions. However, the method is rather suited for high-throughput screening of HDAC inhibitors and the detection of acetylation. Since quantitative assays using

https://doi.org/10.1021/acsomega.0c06281
ACS Omega 2021, 6, 10039−10046

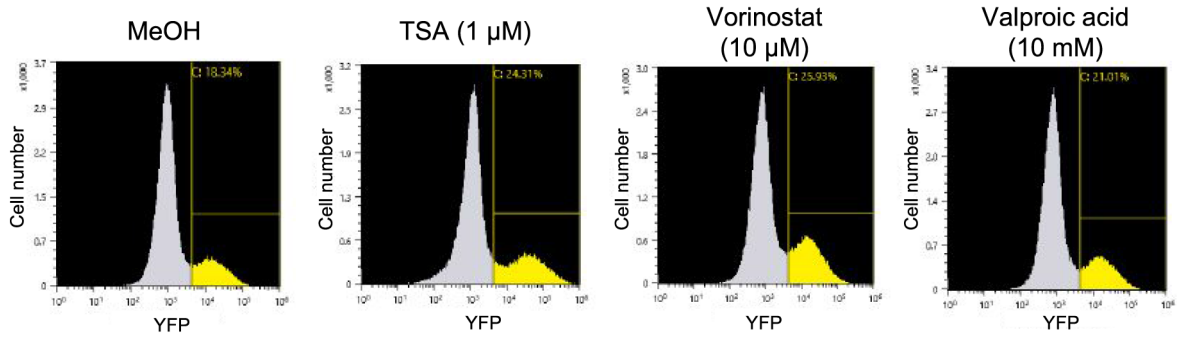

Figure 4. Fluorescence-activated cell sorter (FACS) analysis for detecting YFP signals in Cos-7 cells. Four hours after transfection, the cells were incubated with the vehicle (MeOH), 1 μM TSA, 10 μM vorinostat, or 10 mM valproic acid for 16 h, before harvesting for FACS. The YFP signals reconstituted from the pairing of FP1-10 and CFP-scFv-FP11 are compared. A total of 100 000 cells were analyzed per histogram. Yellow regions were selected as positive. The horizontal and vertical axes indicate the fluorescence intensity derived of YFP and the cell number, respectively. The thin yellow lines indicate the regions set for YFP-positive cell population.

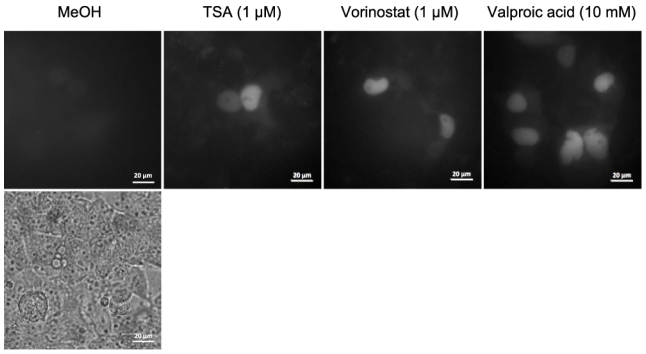

Figure 5. Observation of YFP signals in the nuclei induced by HDAC inhibitor treatments. Four hours after Cos-7 cells were transfected with FP1-10 and APP-scFv-FP11, the cells were incubated with the vehicle (MeOH), 1 μM TSA, 10 μM vorinostat, or 10 mM valproic acid for 16 h, before live imaging. Reconstituted sfYFP signals from the pairing of FP1-10 and APP-scFv-FP11 in the nuclei were detected in the cells treated with HDAC inhibitors.

mintbodies required manual calculations of the nuclear/cytoplasmic fluorescence ratios, it is difficult to be applied to a large number of cells. Although FRET-based probes were barely affected by the expression levels of the probes or bleached by the excitation light, it has some demerits including the measurement of both YPet and CFP signals and the low dynamic range (the change in the FRET index) (<1.5). Compared with these less robust methods, our fluorogenic probe only requires the detection of the YFP signals, have a significantly higher dynamic range (>6), and are applicable to both microscopy and flow cytometry. This simple method enables the rapid and high-throughput screening of HDAC inhibitors in living cells.

There is still room for improvement: (i) the irreversibility of the split-YFP system does not allow the quantitative measurement of acetylation dynamics and (ii) the cell-cycle-dependent release of NLS-FP1-10 from the nucleus via the breakdown of the nuclear envelope induces sfYFP reconstitution after several days. Therefore, the expression period and the expression level need to be characterized. In the future, solutions to overcome these limitations and to expand the method to live cell imaging might include the use of reversible split-FP systems[41,50,51] and/or the addition of degrons.

EXPERIMENTAL SECTION

Plasmid Constructions. To construct a plasmid that expresses the nuclear localization signal (NLS)-FP1-10, the DNA fragment encoding NLS and FP1-10 of the sfYFP sequence, made by introducing respective mutations into YFP,[40] was amplified by polymerase chain reaction (PCR) from the DNA coding sfYFP as the template with the primers InFusion-sfYFPfor and InFusion-FP10rev. The fragment was inserted into pN2-Ypet-scFv(19E5)-ScCFP[33] digested with *Sac*I and *Xba*I using an In-Fusion HD Cloning Kit (Takara-Bio, Shiga, Japan). The nucleotide sequences of primers used are summarized in Table S1. All the restriction enzymes were obtained from New England Biolabs (Ipswich, MA, USA).

To construct a plasmid that expresses the FP11-scFv-CFP, the DNA fragment encoding FP11 of sfYFP was amplified by PCR from the DNA coding sfYFP as the template with the primers InFusion-FP11for and InFusion-sfYFPrev. The fragment was inserted into pN2-Ypet-scFv(19E5)-ScCFP digested with *Nhe*I and *Sac*I using the same In-Fusion Cloning Kit.

To construct a plasmid that expresses the CFP-scFv-FP11, the DNA fragment encoding FP11 of sfYFP was amplified by PCR from the DNA encoding sfYFP as the template with the primers InFusion-BamHI-FP11for and InFusion-XbaI-FP11rev. The fragment was inserted into pN2-FP11-scFv-CFP digested with *Bam*HI and *Xba*I using the same In-Fusion Cloning Kit to yield pN2-FP11-scFv-FP11. The DNA fragment encoding CFP was amplified by PCR from pN2-Ypet-scFv(19E5)-ScCFP as the template with the primers NheI-CFPfor and SacI-CFPrev. The amplified fragment was digested with *Nhe*I and *Sac*I and subcloned into pN2-FP11-scFv-FP11 between *Nhe*I and *Sac*I sites.

To construct the plasmid that expresses the amyloid precursor protein (APP)-FP11-scFv, the DNA fragment encoding FP11 connected to scFv was amplified by PCR with the primers pN2upstream and NotI-stop-mintbody_for. The amplified fragment was digested with *Nhe*I and *Not*I and subcloned into pN2-FP11-CFP between the same sites to yield pN2-FP11-scFv-FP11. The DNA fragment encoding the APP-tag was amplified by PCR from the plasmid encoding a Flashbody[41] with the primers T7 promoter and NheI-APPrev. The amplified fragment was digested with *Nhe*I and subcloned into the *Nhe*I site of pN2-FP11-scFv-FP11.

To construct a plasmid that expresses APP-scFv-FP11, the DNA fragment encoding the APP-tag was amplified by PCR from the plasmid encoding a Flashbody with the primers T7

https://doi.org/10.1021/acsomega.0c06281
ACS Omega 2021, 6, 10039−10046

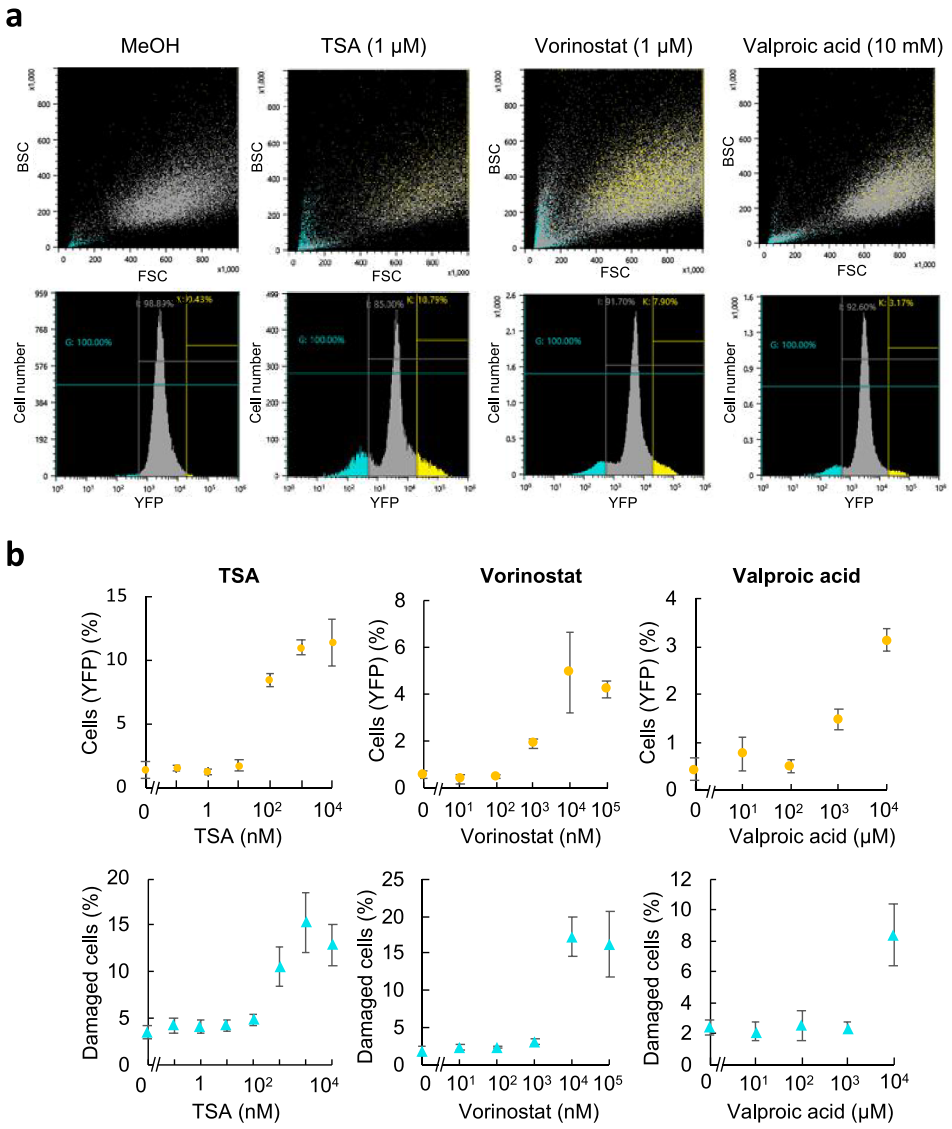

Figure 6. FACS analysis for fluorescent signals and abnormal cells. Four hours after Cos-7 cells were transfected with FP1-10 and APP-scFv-FP11, the cells were incubated with the vehicle (MeOH), 1 μM TSA, 10 μM vorinostat, or 10 mM valproic acid for 16 h, before harvesting for FACS. (a) Histograms of transfected Cos-7 cells with the pairing of FP1-10 and APP-scFv-FP11 when treated with HDAC inhibitors such as TSA, vorinostat, valproic acid, or 0.1% MeOH as a negative control. Upper panels, The horizontal and vertical axes indicate the front scatter (FSC) that reflects the cell size and the back scatter (BSC) that reflects the deformation of the cells, respectively. Lower panels, The horizontal and vertical axes indicate the fluorescence intensity derived of YFP and the cell number, respectively. The thresholds were set for both yellow (YFP-positive) and cyan (damaged) regions so that the lowest detectable concentrations of each HDAC inhibitor were obtained. The thin cyan, gray, and yellow thin lines indicate the regions for all, nondamaged, and YFP-positive cell populations, respectively. (b) The YFP-positive and damaged cell populations (%) calculated from the histograms. More than 4000 cells were analyzed. Data are shown as mean ± standard deviation (n = 3).

promoter and SacI-APPrev. The amplified fragment was digested with *Nhe*I and *Sac*I and subcloned into pN2-CFP-scFv-FP11 between *Nhe*I and *Sac*I sites.

Cell Culture. Cos-7 and U2OS cells were cultured in Dulbecco's modified Eagle's medium (DMEM, Fujifilm Wako Pure Chemical, Osaka, Japan, or Nacalai Tesque, Kyoto, Japan) supplemented with 10% fetal bovine serum (FBS) and Antibiotic−Antimycotic (Gibco, Thermo Fisher, St. Louis, MO, USA) at 37 °C in 5% CO_2 with 100% humidity.

Transfection was performed using Lipofectamine 3000 (Invitrogen, Carlsbad, CA, USA) as per the manufacturer's protocol. Briefly, for a 24-well plate format, 1 μg DNA and 2 μL P3000 solution were mixed in 25 μL Opti-MEM (Thermo Fisher Scientific) and then mixed with 25 μL Opti-MEM containing 1.5 μL Lipofectamine 3000. When two plasmids were mixed, 0.5 μg each was used. After incubation for 15 min, the mixture was added to a well of a 24-well glass-bottom plate (AGC Technology Solutions) containing 0.5 mL medium. After a 4−5 h incubation, the medium containing the plasmids and Lipofectamine 3000 was replaced with FluoBrite DMEM (Thermo Fisher Scientific) supplemented with 10% FBS (Thermo Fisher Scientific) and 1% penicillin−streptomycin−glutamine solution (Sigma-Aldrich), containing methanol (1:1000 dilution), 1 μM trichostatin A (1:1000 dilution from 1 mM stock in methanol; Fujifilm Wako Pure Chemical), 10 μM vorinostat (1:1000 dilution from 10 mM stock in methanol; Tokyo Chemical Industry), or 10 mM valproic acid (1.6:1000 dilution from 6.25 M liquid; Fujifilm Wako Pure Chemical). After incubation for 16−25 h with or without

https://doi.org/10.1021/acsomega.0c06281
ACS Omega 2021, 6, 10039−10046

an inhibitor, the cells were subjected to live cell imaging, immunofluorescence, or cell sorting.

Western Blotting. The cells treated with either MeOH vehicle or each HDAC inhibitor for 16 h were lysed and separated by sodium dodecyl sulphate−polyacrylamide gel electrophoresis (SDS−PAGE), before transferring onto a nitrocellulose membrane. The separated membranes were washed thrice with TBST, blocked for 1 h in 1% skim milk in TBST, and incubated for 1 h at 25 °C with rat anti-H3 (1:20 000), mouse anti-H3K9Ac (1:2000), or mouse anti-GFP antibody (1:100) (Wako) in TBST. The membranes were washed thrice with TBST and incubated for 30 min at 25 °C with either HRP-goat anti-rat IgG(H + L) (1:5000) (SeraCare, Milford, MA, USA) or HRP-rabbit anti-mouse IgG2a (1:2000) in PBST. Signals were developed as above using a luminescent imager LuminoGraphII (ATTO, Tokyo, Japan).

Immunostaining. Twenty-two hours after HDAC treatment, the cells were fixed with 4% paraformaldehyde in 250 mM HEPES (*N*-(2-hydroxyethyl)piperazine-*N*′-ethanesulfonic acid), pH 7.4, for 5 min. After washing three times with phosphate-buffered saline (PBS), the cells were treated with 1% Triton X-100 in PBS for 20 min and blocked with Blocking One-P (Nacalai Tesque, Kyoto, Japan) for 20 min. After washing three times with PBS, the cells were stained with anti H3K9ac CMA310 antibody conjugated with Cy5 (1.5 μg/mL)[42] overnight and washed with PBS.

Fluorescence Intensity Assessment. The fluorescence intensities of YFP and CFP were collected either by fluorescence microscopy (IX71, Olympus, Tokyo, Japan) or by confocal microscopy FV1000 (Olympus) equipped with a PlanApo N 60× Oil SC lens (NA 1.40; Olympus). The former images were taken with 0.5 s exposure time and a sensitivity gain of 50 using the HCImage system equipped with an ImagEM EM-CCD camera (Hamamatsu Photonics, Shizuoka, Japan). The differential interference contrast image was captured with 50 ms exposure time and a sensitivity gain of 5. The confocal microscopic images were collected using an FV1000 under the operation with Olympus FV10-ASW 4.2 software using a confocal aperture 100 μm, a scan speed 4.0 μs/pixel, line average 4×, zoom 3×, and a frame size 512 × 512 pixels (0.138 μm/pixel). CFP and YFP signals were detected with a line sequential image acquisition mode using 458 and 515 nm laser lines (each 5% or 10% transmission for Cos-7 or U2OS) and with a DM458/515 dichroic mirror and BA480-495 and BA535-565 bandpass filters. A transmission detector was also used when necessary. For immunofluorescence, images were acquired sequentially with 458, 515, and 633 nm laser excitations with 16.5%, 45.2%, and 3.5% transmissions, respectively, with a confocal aperture 200 μm, a scan speed 4.0 μs/pixel (0.051 μm/pixel), zoom 4×, and a line average 4×.

The nuclear YFP fluorescence/total cellular CFP fluorescence intensity ratios were calculated as described previously[33] with slight modification. Briefly, the fluorescence intensities of nuclear and total cellular regions were manually selected as regions of interest (ROIs) and quantified using ImageJ (NIH, Bethesda, MD). The fluorescence intensities were quantified by drawing ROIs within the nuclei and cells.

Flow cytometric analysis was performed using an SH-800 cell sorter (Sony, Tokyo, Japan). YFP was excited at 488 nm, and the emission was detected through a 525 nm/50 nm bandpass filter as green fluorescence.

■ ASSOCIATED CONTENT

Supporting Information

The Supporting Information is available free of charge at https://pubs.acs.org/doi/10.1021/acsomega.0c06281.

Table S1 for primer sequences; figures for the box plot of the nuclear YFP/total cellular CFP fluorescence intensity ratios, FACS analysis for the cells without transfection, western blot analysis of the expressed probes, observation of YFP signals using APP-fused probes, and positive correlation of the YFP positive- and damaged-cell populations (PDF)

■ AUTHOR INFORMATION

Corresponding Author

Hiroshi Ueda − *Laboratory for Chemistry and Life Science, Tokyo Institute of Technology, Yokohama, Kanagawa 226-8503, Japan;* orcid.org/0000-0001-8849-4217; Email: ueda@res.titech.ac.jp

Authors

Yuki Ohmuro-Matsuyama − *Laboratory for Chemistry and Life Science, Tokyo Institute of Technology, Yokohama, Kanagawa 226-8503, Japan; Technology Research Laboratory, Shimadzu Corporation, Kyoto 619-0237, Japan*

Tetsuya Kitaguchi − *Laboratory for Chemistry and Life Science, Tokyo Institute of Technology, Yokohama, Kanagawa 226-8503, Japan;* orcid.org/0000-0001-6701-1933

Hiroshi Kimura − *Cell Biology Center, Institute of Innovative Research, Tokyo Institute of Technology, Yokohama, Kanagawa 226-8503, Japan;* orcid.org/0000-0003-0854-083X

Complete contact information is available at: https://pubs.acs.org/10.1021/acsomega.0c06281

Author Contributions

Y.O.-M designed and carried out the experiments and wrote the manuscript draft. H.U. conceived the study and wrote the manuscript with the inputs from all authors. H.K. supplied the intrabody gene and performed the experiments. T.K. provided sfYFP gene and supported the experiments. All authors have given approval to the final version of the manuscript.

Funding

This work was supported in part by JSPS KAKENHI—Grant nos. JP18H03851 (to H.U.), JP17K06920 (to Y.O.-M), and JP18H05527 (to H.K.) from the Japan Society for the Promotion of Science, Japan; by JST-Mirai—Grant No. JPMJMI18D9 (to H.U.) from Japan Science and Technology Agency, Japan; and the research fund from Shimadzu Corporation (to Y.O.-M.).

Notes

The authors declare no competing financial interest.

■ ACKNOWLEDGMENTS

We thank Chiaki Toyama for the experimental help, the Biomaterials Analysis Division, Open Facility Center, Tokyo Institute of Technology for DNA sequence analysis, and the support by Dynamic Alliance for Open Innovation Bridging Human, Environment and Materials from MEXT, Japan.

REFERENCES

(1) Chen, Z.; Li, W.; Qiu, F.; Huang, Q.; Jiang, Z.; Ye, J.; Cheng, P.; Low, C.; Guo, Y.; Yi, X.; Chen, W.; Yu, Y.; Han, Y.; Wu, J.; Jin, S.; Kong, D.; Huang, J. Aspirin cooperates with p300 to activate the acetylation of H3K9 and promote FasL-mediated apoptosis of cancer stem-like cells in colorectal cancer. *Theranostics* **2018**, *8*, 4447−4461.

(2) Eckschlager, T.; Plch, J.; Stiborova, M.; Hrabeta, J. Histone deacetylase inhibitors as anticancer drugs. *Int. J. Mol. Sci.* **2017**, *18*, 1414.

(3) Falkenberg, K. J.; Johnstone, R. W. Histone deacetylases and their inhibitors in cancer, neurological diseases and immune disorders. *Nat. Rev. Drug Discovery* **2014**, *13*, 673−691.

(4) Gao, X.; Lin, S. H.; Ren, F.; Li, J. T.; Chen, J. J.; Yao, C. B.; Yang, H. B.; Jiang, S. X.; Yan, G. Q.; Wang, D.; Wang, Y.; Liu, Y.; Cai, Z.; Xu, Y. Y.; Chen, J.; Yu, W.; Yang, P. Y.; Lei, Q. Y. Acetate functions as an epigenetic metabolite to promote lipid synthesis under hypoxia. *Nat. Commun.* **2016**, *7*, No. 11960.

(5) Judes, G.; Dagdemir, A.; Karsli-Ceppioglu, S.; Lebert, A.; Echegut, M.; Ngollo, M.; Bignon, Y. J.; Penault-Llorca, F.; Bernard-Gallon, D. H3K4 acetylation, H3K9 acetylation and H3K27 methylation in breast tumor molecular subtypes. *Epigenomics* **2016**, *8*, 909−924.

(6) Wisnieski, F.; Leal, M. F.; Calcagno, D. Q.; Santos, L. C.; Gigek, C. O.; Chen, E. S.; Artigiani, R.; Demachki, S.; Assumpcao, P. P.; Lourenco, L. G.; Burbano, R. R.; Smith, M. C. BMP8B is a tumor suppressor gene regulated by histone acetylation in gastric cancer. *J. Cell. Biochem.* **2017**, *118*, 869−877.

(7) Xu, Y.; Qin, L.; Sun, T.; Wu, H.; He, T.; Yang, Z.; Mo, Q.; Liao, L.; Xu, J. Twist1 promotes breast cancer invasion and metastasis by silencing Foxa1 expression. *Oncogene* **2017**, *36*, 1157−1166.

(8) Patnala, R.; Arumugam, T. V.; Gupta, N.; Dheen, S. T. HDAC inhibitor sodium butyrate-mediated epigenetic regulation enhances neuroprotective function of microglia during ischemic stroke. *Mol. Neurobiol.* **2017**, *54*, 6391−6411.

(9) Bustos, F. J.; Ampuero, E.; Jury, N.; Aguilar, R.; Falahi, F.; Toledo, J.; Ahumada, J.; Lata, J.; Cubillos, P.; Henriquez, B.; Guerra, M. V.; Stehberg, J.; Neve, R. L.; Inestrosa, N. C.; Wyneken, U.; Fuenzalida, M.; Hartel, S.; Sena-Esteves, M.; Varela-Nallar, L.; Rots, M. G.; Montecino, M.; Van Zundert, B. Epigenetic editing of the Dlg4/PSD95 gene improves cognition in aged and Alzheimer's disease mice. *Brain* **2017**, *140*, 3252−3268.

(10) Tago, T.; Toyohara, J. Advances in the development of PET ligands targeting histone deacetylases for the assessment of neurodegenerative diseases. *Molecules* **2018**, *23*, 300.

(11) Ganai, S. A.; Ramadoss, M.; Mahadevan, V. Histone Deacetylase (HDAC) Inhibitors—Emerging roles in neuronal memory, learning, synaptic plasticity and neural regeneration. *Curr. Neuropharmacol.* **2016**, *14*, 55−71.

(12) Kidd, C. D.; Thompson, P. J.; Barrett, L.; Baltic, S. Histone modifications and asthma. The interface of the epigenetic and genetic landscapes. *Am. J. Respir. Cell Mol. Biol.* **2016**, *54*, 3−12.

(13) Ren, Y.; Su, X.; Kong, L.; Li, M.; Zhao, X.; Yu, N.; Kang, J. Therapeutic effects of histone deacetylase inhibitors in a murine asthma model. *Inflammation Res.* **2016**, *65*, 995−1008.

(14) Brook, P. O.; Perry, M. M.; Adcock, I. M.; Durham, A. L. Epigenome-modifying tools in asthma. *Epigenomics* **2015**, *7*, 1017−1032.

(15) Royce, S. G.; Karagiannis, T. C. Histone deacetylases and their inhibitors: New implications for asthma and chronic respiratory conditions. *Curr. Opin. Allergy Clin. Immunol.* **2014**, *14*, 44−48.

(16) Daiwile, A. P.; Sivanesan, S.; Tarale, P.; Naoghare, P. K.; Bafana, A.; Parmar, D.; Kannan, K. Role of fluoride induced histone trimethylation in development of skeletal fluorosis. *Environ. Toxicol. Pharmacol.* **2018**, *57*, 159−165.

(17) Daiwile, A. P.; Tarale, P.; Sivanesan, S.; Naoghare, P. K.; Bafana, A.; Parmar, D.; Kannan, K. Role of fluoride induced epigenetic alterations in the development of skeletal fluorosis. *Ecotoxicol. Environ. Saf.* **2019**, *169*, 410−417.

(18) Wu, S.; Yan, W.; Qiu, B.; Liao, Y.; Gu, J.; Wei, S.; Zhang, A.; Pan, X. Aberrant methylation-induced dysfunction of p16 is associated with osteoblast activation caused by fluoride. *Environ. Toxicol.* **2019**, *34*, 37−47.

(19) Ming, J.; Wu, S.; You, T.; Wang, X.; Yu, C.; Luo, P.; Zhang, A.; Pan, X. Histone deacetylation in the promoter of p16 is involved in fluoride-induced human osteoblast activation via the inhibition of Sp1 binding. *Biol. Trace Elem. Res.* **2019**, *188*, 373−383.

(20) Klein, H. U.; McCabe, C.; Gjoneska, E.; Sullivan, S. E.; Kaskow, B. J.; Tang, A.; Smith, R. V.; Xu, J.; Pfenning, A. R.; Bernstein, B. E.; Meissner, A.; Schneider, J. A.; Mostafavi, S.; Tsai, L. H.; Young-Pearse, T. L.; Bennett, D. A.; De Jager, P. L. Epigenome-wide study uncovers large-scale changes in histone acetylation driven by tau pathology in aging and Alzheimer's human brains. *Nat. Neurosci.* **2019**, *22*, 37−46.

(21) Jung, E. M.; Moffat, J. J.; Liu, J.; Dravid, S. M.; Gurumurthy, C. B.; Kim, W. Y. Arid1b haploinsufficiency disrupts cortical interneuron development and mouse behavior. *Nat. Neurosci.* **2017**, *20*, 1694−1707.

(22) Coppede, F. The potential of epigenetic therapies in neurodegenerative diseases. *Front. Genet.* **2014**, *5*, 220.

(23) Li, Y.; Seto, E. HDACs and HDAC inhibitors in cancer development and therapy. *Cold Spring Harbor Perspect. Med.* **2016**, *6*, No. a026831.

(24) Kimura, H.; Hayashi-Takanaka, Y.; Stasevich, T. J.; Sato, Y. Visualizing posttranslational and epigenetic modifications of endogenous proteins in vivo. *Histochem. Cell Biol.* **2015**, *144*, 101−109.

(25) Sasaki, K.; Ito, A.; Yoshida, M. Development of live-cell imaging probes for monitoring histone modifications. *Bioorg. Med. Chem.* **2012**, *20*, 1887−1892.

(26) Nakaoka, S.; Sasaki, K.; Ito, A.; Nakao, Y.; Yoshida, M. A genetically encoded FRET probe to detect intranucleosomal histone H3K9 or H3K14 acetylation using BRD4, a BET family member. *ACS Chem. Biol.* **2016**, *11*, 729−733.

(27) Kobayashi, H.; Choyke, P. L.; Ogawa, M. Monoclonal antibody-based optical molecular imaging probes: Considerations and caveats in chemistry, biology and pharmacology. *Curr. Opin. Chem. Biol.* **2016**, *33*, 32−38.

(28) Lyon, K.; Stasevich, T. J. Imaging translational and post-translational gene regulatory dynamics in living cells with antibody-based probes. *Trends Genet.* **2017**, *33*, 322−335.

(29) Guglielmi, L.; Martineau, P. Intrabody expression in eukaryotic cells. *Methods Mol. Biol.* **2009**, *562*, 195−203.

(30) Sato, Y.; Mukai, M.; Ueda, J.; Muraki, M.; Stasevich, T. J.; Horikoshi, N.; Kujirai, T.; Kita, H.; Kimura, T.; Hira, S.; Okada, Y.; Hayashi-Takanaka, Y.; Obuse, C.; Kurumizaka, H.; Kawahara, A.; Yamagata, K.; Nozaki, N.; Kimura, H. Genetically encoded system to track histone modification in vivo. *Sci. Rep.* **2013**, *3*, No. 2436.

(31) Suzuki, M.; Takagi, C.; Miura, S.; Sakane, Y.; Suzuki, M.; Sakuma, T.; Sakamoto, N.; Endo, T.; Kamei, Y.; Sato, Y.; Kimura, H.; Yamamoto, T.; Ueno, N.; Suzuki, K. T. In vivo tracking of histone H3 lysine 9 acetylation in Xenopus laevis during tail regeneration. *Genes Cells* **2016**, *21*, 358−369.

(32) Sato, Y.; Kujirai, T.; Arai, R.; Asakawa, H.; Ohtsuki, C.; Horikoshi, N.; Yamagata, K.; Ueda, J.; Nagase, T.; Haraguchi, T.; Hiraoka, Y.; Kimura, A.; Kurumizaka, H.; Kimura, H. A genetically encoded probe for live-cell imaging of H4K20 monomethylation. *J. Mol. Biol.* **2016**, *428*, 3885−3902.

(33) Chung, C. I.; Sato, Y.; Ohmuro-Matsuyama, Y.; Machida, S.; Kurumizaka, H.; Kimura, H.; Ueda, H. Intrabody-based FRET probe to visualize endogenous histone acetylation. *Sci. Rep.* **2019**, *9*, No. 10188.

(34) Romei, M. G.; Boxer, S. G. Split green fluorescent proteins: Scope, limitations, and outlook. *Annu. Rev. Biophys.* **2019**, *48*, 19−44.

(35) Avitabile, E.; Forghieri, C.; Campadelli-Fiume, G. Complexes between herpes simplex virus glycoproteins gD, gB, and gH detected in cells by complementation of split enhanced green fluorescent protein. *J. Virol.* **2007**, *81*, 11532−11537.

https://doi.org/10.1021/acsomega.0c06281
ACS Omega 2021, 6, 10039−10046

(36) Magliery, T. J.; Wilson, C. G.; Pan, W.; Mishler, D.; Ghosh, I.; Hamilton, A. D.; Regan, L. Detecting protein−protein interactions with a green fluorescent protein fragment reassembly trap: Scope and mechanism. *J. Am. Chem. Soc.* **2005**, *127*, 146−157.
(37) Morell, M.; Espargaro, A.; Aviles, F. X.; Ventura, S. Detection of transient protein−protein interactions by bimolecular fluorescence complementation: The Abl-SH3 case. *Proteomics* **2007**, *7*, 1023−1036.
(38) Cabantous, S.; Nguyen, H. B.; Pedelacq, J. D.; Koraichi, F.; Chaudhary, A.; Ganguly, K.; Lockard, M. A.; Favre, G.; Terwilliger, T. C.; Waldo, G. S. A new protein−protein interaction sensor based on tripartite split-GFP association. *Sci. Rep.* **2013**, *3*, No. 2854.
(39) Cabantous, S.; Terwilliger, T. C.; Waldo, G. S. Protein tagging and detection with engineered self-assembling fragments of green fluorescent protein. *Nat. Biotechnol.* **2005**, *23*, 102−107.
(40) Gan, L.; Ni, P. Y.; Ge, Y.; Xiao, Y. F.; Sun, C. Y.; Deng, L.; Zhang, W.; Wu, S. S.; Liu, Y.; Jiang, W.; Xin, H. B. Histone deacetylases regulate gonadotropin-releasing hormone I gene expression via modulating Otx2-driven transcriptional activity. *PLoS One* **2012**, *7*, No. e39770.
(41) Hayashi-Takanaka, Y.; Kina, Y.; Nakamura, F.; Becking, L. E.; Nakao, Y.; Nagase, T.; Nozaki, N.; Kimura, H. Histone modification dynamics as revealed by multicolor immunofluorescence-based single-cell analysis. *J. Cell. Sci.* **2020**, *133*, No. jcs243444.
(42) Johansson, A. S.; Brask, J.; Owe-Larsson, B.; Hetta, J.; Lundkvist, G. B. Valproic acid phase shifts the rhythmic expression of Period2::Luciferase. *J. Biol. Rhythms* **2011**, *26*, 541−551.
(43) Gross, L. A.; Baird, G. S.; Hoffman, R. C.; Baldridge, K. K.; Tsien, R. Y. The structure of the chromophore within DsRed, a red fluorescent protein from coral. *Proc. Natl. Acad. Sci. U.S.A.* **2000**, *97*, 11990−11995.
(44) Barondeau, D. P.; Kassmann, C. J.; Tainer, J. A.; Getzoff, E. D. Understanding GFP posttranslational chemistry: Structures of designed variants that achieve backbone fragmentation, hydrolysis, and decarboxylation. *J. Am. Chem. Soc.* **2006**, *128*, 4685−4693.
(45) Nakatani, T.; Yasui, N.; Tamura, I.; Yamashita, A. Specific modification at the C-terminal lysine residue of the green fluorescent protein variant, GFPuv, expressed in *Escherichia coli*. *Sci. Rep.* **2019**, *9*, No. 4722.
(46) Sangawa, T.; Tabata, S.; Suzuki, K.; Saheki, Y.; Tanaka, K.; Takagi, J. A multipurpose fusion tag derived from an unstructured and hyperacidic region of the amyloid precursor protein. *Protein Sci.* **2013**, *22*, 840−850.
(47) Wongso, D.; Dong, J.; Ueda, H.; Kitaguchi, T. Flashbody: A next generation fluobody with fluorescence intensity enhanced by antigen binding. *Anal. Chem.* **2017**, *89*, 6719−6725.
(48) Tchekanda, E.; Sivanesan, D.; Michnick, S. W. An infrared reporter to detect spatiotemporal dynamics of protein-protein interactions. *Nat. Methods* **2014**, *11*, 641−644.
(49) To, T. L.; Zhang, Q.; Shu, X. Structure-guided design of a reversible fluorogenic reporter of protein−protein interactions. *Protein Sci.* **2016**, *25*, 748−753.
(50) Pédelacq, J.-D.; Cabantous, S.; Tran, T.; Terwilliger, T. C.; Waldo, G. S. Engineering and characterization of a superfolder green fluorescent protein. *Nat. Biotechnol.* **2006**, *24*, 79−88.
(51) Kimura, H.; Hayashi-Takanaka, Y.; Goto, Y.; Takizawa, N.; Nozaki, N. The organization of histone H3 modifications as revealed by a panel of specific monoclonal antibodies. *Cell Struct. Funct.* **2008**, *33*, 61−73.

https://doi.org/10.1021/acsomega.0c06281
ACS Omega 2021, 6, 10039−10046